Fatigue Characteristics of High-Speed Train Axles with Different Prefabricated Surface Notches

Chun Gao , Zhengwei Yu , Shisen Liu , Yuanyuan Zhang , Tao Fan , Hang Su *

Posted Date: 2 July 2025

doi: 10.20944/preprints202507.0178.v1

Keywords: high-speed train axles; prefabricated surface notches; circumferential V-shaped notches; fatigue characteristics; stress concentration factor (SCF); fatigue testing; magnetic particle inspection; notch depth; fatigue strength; overhaul specifications

 doi:10.20944/preprints202507.0178.v1

Article

Fatigue Characteristics of High-Speed Train Axles with Different Prefabricated Surface Notches

Chun Gao [1,2], Zhengwei Yu [3], Shisen Liu [4], Yuanyuan Zhang [1], Tao Fan [5] and Hang Su [6,*]

[1] School of Civil Engineering, Harbin University, Harbin 150086, China
[2] Heilongjiang Province Key Laboratory of Underground Engineering Technology, Harbin University, Harbin 150086, China
[3] College of Science, Heilongjiang University of Science and Technology, Harbin 150020, China
[4] School of Electronic Information, Chongqing Institute of Engineering, Chongqing 400056, China
[5] Heilongjiang Zhongbei Post and Telecommunications Construction and Development Company, Harbin 150036, China
[6] Department of Civil Engineering, University of California, Los Angeles, CA 90095, USA
* Correspondence: hangsu2018@g.ucla.edu

Abstract

High-speed train axles with prefabricated surface notches are critical for evaluating fatigue resistance under cyclic loading. This study investigates the fatigue characteristics of axles with circumferential V-shaped notches of varying depths (0.538–1.760 mm) and stress concentration factors (2.48–5.49). Fatigue tests were conducted at 19.8 Hz with a stress ratio of −1, up to 2×10^7 cycles, following EN 13261 standards. Magnetic particle inspection revealed no crack initiation in notched segments, even at maximum local stresses reaching 1082.8 MPa. Results demonstrate excellent fatigue resistance of axle materials, with deeper notches (up to 1.760 mm) still maintaining integrity. The findings challenge conservative overhaul specifications (allowing impact depth less than 0.3 mm), suggesting potential relaxation based on experimental evidence. This work highlights the need for comprehensive fatigue assessment beyond local stress concentration alone.

Keywords: high-speed train axles; prefabricated surface notches; circumferential V-shaped notches; fatigue characteristics; stress concentration factor (SCF); fatigue testing; magnetic particle inspection; notch depth; fatigue strength; overhaul specifications

1. Introduction

High-speed train axles play a critical role in ensuring the safety and reliability of modern rail transportation systems [1–6], as they are subjected to complex cyclic loading conditions that include bending, torsion [7], and dynamic impacts during operation. The fatigue performance of these axles, particularly when featuring prefabricated surface notches [8–13] that simulate real-world defects such as fretting damage [14–17] or impact-induced flaws [18–20], has become a focal point of research due to the increasing demands of higher operational speeds and heavier loads. Specimen surface or surface notches are known to act as primary initiation sites for fatigue cracks [21–23], potentially leading to catastrophic failures if not properly understood and managed. Despite the importance of this issue, existing industry standards such as EN 13261 [24] provide limited guidance on the specific relationship between notch geometry (e.g., depth, tip radius, angle) and the fatigue life of full-scale axles, while maintenance specifications often adopt conservative limits for allowable damage (e.g., maximum impact depth of 0.3 mm) that may not fully reflect the actual fatigue resistance of axle materials [8–13,25].

Numerous studies [8–13,26–36] have investigated the fatigue behavior of notched components, but most have focused on small-scale specimens or simplified notch configurations, failing to fully capture the complex three-dimensional stress states and boundary conditions present in full-size

 doi:10.20944/preprints202507.0178.v1

train axles. For instance, research on the fatigue properties of axle materials like S38C steel has typically relied on standard test specimens under rotating bending, overlooking the influence of wheel-seat interactions and dynamic loading scenarios that characterize real-world axle operation [11,37–40]. Additionally, circumferential V-shaped notches, which more accurately mimic the sharp defects caused by fretting or impact in service, have received limited attention in prior studies, with most investigations focusing on U-shaped or other notch geometries. This gap in knowledge is further compounded by the lack of specific fatigue limit testing protocols for full-scale axles in standards such as JIS E4501, leading to uncertainties in engineering assessments of axle integrity and service life [41].

The relationship between very high cycle fatigue (VHCF [42–59]) and railway axles is critical for ensuring long-term reliability, as axles endure billions of cyclic loads during service, often exceeding 10^7 cycles in the VHCF regime. In this context, VHCF failures typically stem from internal defects like non-metallic inclusions or micro-voids within the axle material, which act as stress concentrators and trigger crack initiation beneath the surface. Characteristic "fish-eye" fracture patterns emerge, with inclusions at the core surrounded by a granular bright facet zone, highlighting the role of microstructural inhomogeneities in crack propagation. Key influencing factors include material purity, inclusion size/distribution, and surface treatments—such as shot peening or induction hardening—that mitigate stress concentrations and suppress crack growth. Understanding this VHCF-axle relationship is essential for refining design standards (e.g., EN 13261) and inspection protocols to prevent unexpected failures and enhance the service life of railway components. Additive manufacturing [60–66] enables the fabrication of railway axles with optimized microstructures and tailored notch reinforcements, enhancing fatigue resistance and enabling complex geometries unattainable via traditional methods.

The primary objective of this study is to systematically investigate the fatigue characteristics of high-speed train axles featuring prefabricated circumferential V-shaped notches with varying depths and stress concentration factors (SCFs). By conducting experimental tests on actual axles, the research aims to: (1) evaluate the impact of notch depth (ranging from 0.538 to 1.760 mm) and SCF (2.48 to 5.49) on axle fatigue life under cyclic loading with a stress ratio of $R = -1$ and up to 2×10^7 cycles; (2) validate the fatigue resistance of axles with notches deeper than current maintenance thresholds, providing empirical data to inform potential revisions to conservative maintenance specifications; and (3) challenge the conventional assumption that fatigue strength can be solely determined by the local maximum stress at the notch root, thereby promoting a more comprehensive approach to fatigue assessment.

The study employs a wheel-axle test bench to apply controlled cyclic loading at a frequency of 19.8 Hz, in accordance with the EN 13261 standard, while magnetic particle inspection is used to monitor crack initiation at the prefabricated notches. Replica techniques and optical microscopy are utilized to precisely characterize the geometry of the notches, including their depth, opening angle, and tip radius of curvature, allowing for accurate calculation of SCFs. By progressively deepening the notches and subjecting the axles to increasing numbers of loading cycles, the research seeks to establish a quantitative relationship between notch severity and fatigue performance, bridging the gap between laboratory-scale studies and real-world engineering applications.

The findings of this study are expected to contribute to a deeper understanding of the fatigue mechanisms governing notched axles, providing critical insights for the design, maintenance, and inspection of high-speed train components. By demonstrating the fatigue resistance of axles with notches exceeding traditional damage limits, the research may also inform the development of more efficient and evidence-based maintenance strategies, ultimately enhancing the safety and operational efficiency of high-speed rail systems worldwide. The subsequent sections of this paper will detail the experimental methods, present the results of the fatigue tests, discuss the implications of the findings in the context of existing standards and theories, and conclude with recommendations for future research in this field.

 doi:10.20944/preprints202507.0178.v1

2. Materials and Methods

2.1. Test Bench

In this research, fretting or impact damage defects were approximately modeled as circumferential V-shaped notches encircling the axle body. To intensify stress concentration, the notch depth and sharpness were increased, and the distance between the notch and the wheel seat was reduced. These modifications were introduced to further investigate, through fatigue testing, the fatigue performance of actual high-speed train axles with various prefabricated surface notches.

The axle fatigue tests were conducted on the wheel-axle test bench as shown in Figure 1. The tests were carried out at a loading frequency of 19.8 Hz, with a stress ratio of R = -1, and the total number of loading cycles was set to no less than 2×10^7 cycles. After each 10^7-cycle interval, magnetic particle inspection was performed to examine whether cracks had initiated at the artificially introduced notch on the axle body.

Since the JIS E4501-1995 standard does not specify the fatigue limit or testing method for actual axles, the maximum load in the present fatigue experiments was determined according to the EN 13261 standard, setting the maximum applied stress at 240 MPa.

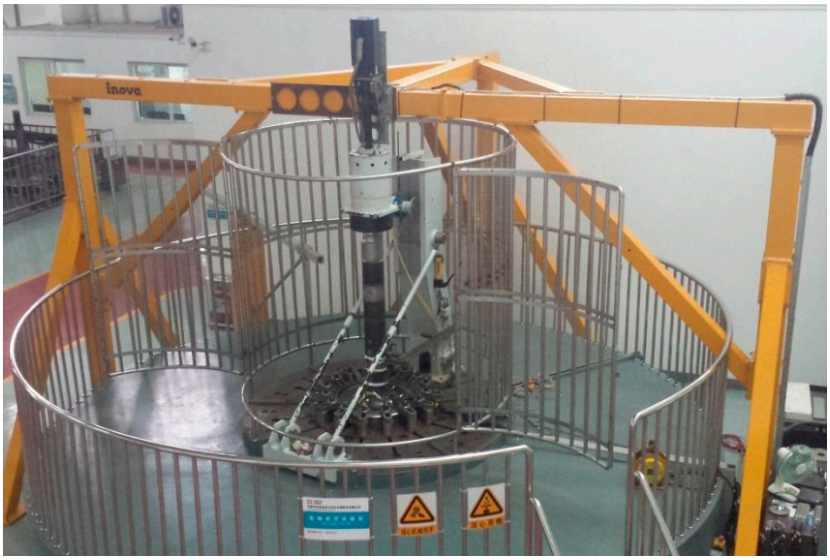

Figure 1. The test bench is equipped with an experimental high-speed train axle.

2.2. Prefabrication of Surface Notches

Based on the observed data of impact and fretting damage on axle surfaces, as well as the fatigue test results which investigated actual axles with circumferential V-shaped notches and the fatigue strength tests of notched three-point bending specimens directly extracted from the axle surface material, two actual axles were selected for testing (Axle Nos.: H31-6201 and H82-6217). The following circumferential V-shaped notches were designed and introduced on these axles: distance from the notch to the wheel seat 130 mm, notch angle $\alpha = 90°$, notch depth $t = 0.6$ mm, notch tip radius of curvature ρ = 0.4 mm, stress concentration factor k_{t0} = 2.49. Based on the measured stress at the patch locations on cross-sections of the axles, and elastic beam theory, the maximum nominal bending stress at the V-shaped notch is calculated to be 220.2 MPa.

The location of the prefabricated artificial notch is illustrated in Figure 2a, and the machined notch produced by lathe processing is shown in Figures 2b–c.

 doi:10.20944/preprints202507.0178.v1

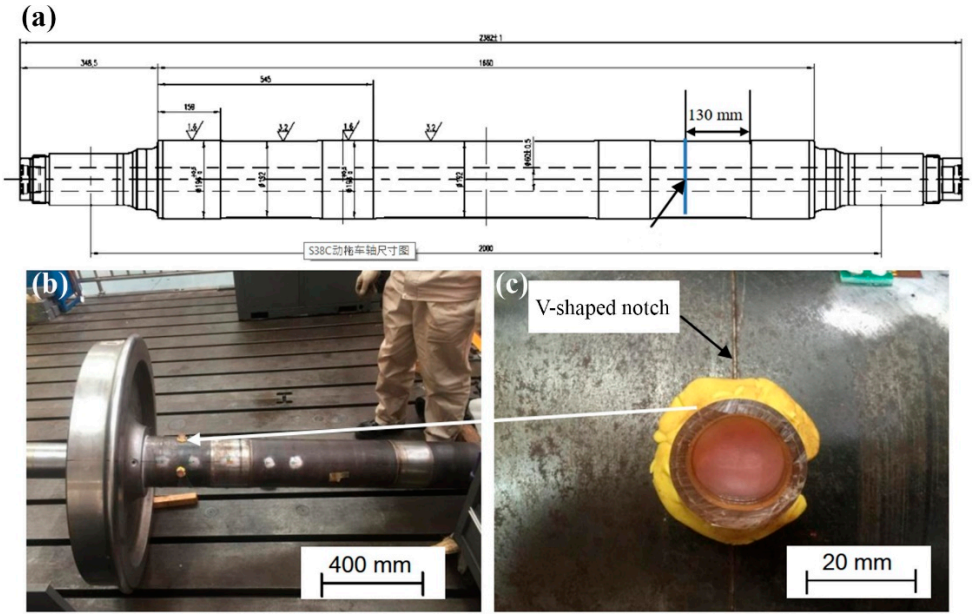

Figure 2. Prefabrication of surface notches: (a) schematic of prefabricated notch location, (b) V-shaped notch on the testing axle, (c) replica sampling of the notch.

The replica technique was employed to replicate the morphology of the V-shaped notch. An optical microscope was used to measure the profile of the replica sample, allowing for the determination of the actual geometric dimensions of the prefabricated artificial notch.

The geometric parameters of the V-shaped notch are illustrated in Figure 3, and the notch angle α and dimension x were calculated using Equations (1) and (2).

$$\alpha = \frac{360}{\pi}\arctan\left(\frac{r}{x}\right) = \frac{360}{\pi}\arctan\left(\frac{c}{2\left(t-r+\sqrt{r^2+x^2}\right)}\right) \quad (1)$$

$$\frac{r}{x} = \frac{c}{2\left(t-r+\sqrt{r^2+x^2}\right)} \quad (2)$$

The radius of curvature at the notch tip was determined by performing a quadratic curve fitting using several measurement points selected from the tip region of the V-shaped notch. The corresponding calculation is based on the following equation:

$$\rho = \left|\frac{\left[1+\left(\frac{dy}{dx}\right)^2\right]^{3/2}}{\frac{d^2y}{dx^2}}\right| \quad (3)$$

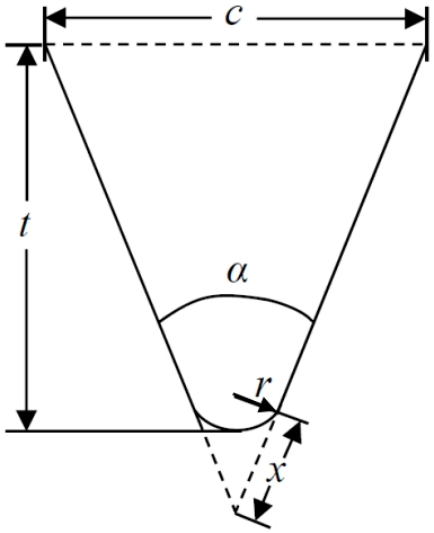

Figure 3. Schematic of a V-shaped notch with the parameters r, c, t, and x.

 doi:10.20944/preprints202507.0178.v1

3. Results

3.1. 1st Round Fatigue Test and Results

Figure 4 presents the results for Axle H31-6201 with prefabricated notches, including replica profile photographs of the notches (Figure 4a), measured geometric dimensions of the notches and quadratic curve fitting results used to evaluate the notch tip curvature (Figure 4b).

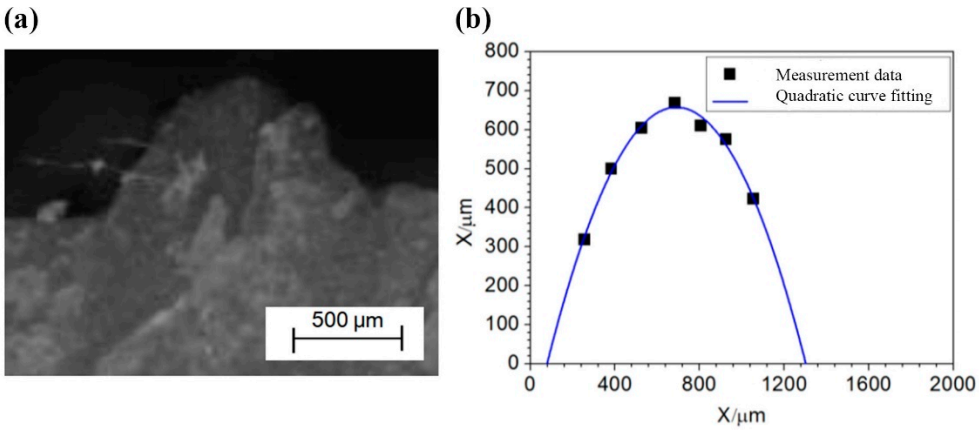

Figure 4. V-shape notch on Axle H31-6201: (a) optical observation of the replica profile, (b) quadratic curve fitting.

The actual geometric parameters of the axle notches obtained from the replicas, along with the corresponding stress concentration factors, are summarized in Table 1.

Table 1. Dimensions of notches and corresponding stress concentration factors (SCF).

Axle number	Notch opening angle	Notch depth/mm	Curvature radius at the notch base	SCF
H82-6217	88.6°	0.572	0.389	2.48
H31-6201	86.0°	0.538	0.355	2.53

Since all the two axles had previously undergone a baseline wheel seat fatigue test at 94 MPa for 10^7 cycles, the current tests were conducted in a stepwise manner.

For Axle H82-6217, a 136 MPa shaft fatigue test was first carried out. Upon confirming the absence of abnormalities, a 240 MPa fatigue test was subsequently performed. Based on the results and experience gained from the first axles, Axle H31-6201 was subjected directly to the 240 MPa fatigue test. The experimental results are summarized in Table 2.

Table 2. Axle test results.

Axle number	Loading/MPa	Number of cycles	Test result description
H82-6217	Axle body 136	1×10^7	No cracks detected (low-load preliminary test)
	Axle body 240	1×10^7	No cracks detected
		1×10^7	No cracks detected
H31-6201	Axle body 240	1×10^7	No cracks detected
		1×10^7	No cracks detected

3.2. 2nd Round Fatigue Test and Results (Notch Deepened)

Based on the results of the first round of testing, one of the axles, Axle H82-6217, was selected for further modification. Specifically, the original V-shaped notch was deepened at eight circumferentially symmetric positions using a riffler file, aiming for a maximum notch depth of

 doi:10.20944/preprints202507.0178.v1

approximately 1.0 mm. The maximum nominal bending stress at the notch location was determined to be 220.2 MPa.

The replica technique was employed to reproduce the actual morphology of the notches at eight locations around the circumference. The profiles of the replica samples were then examined using an optical microscope, enabling the measurement of the actual geometric dimensions of the artificially prefabricated notches. The notch opening angle α was calculated using Equation (1), while the notch tip radius of curvature was determined by selecting several measurement points near the notch tip, applying quadratic curve fitting, and using Equation (3).

Figure 5 presents the results of one of the eight notches on Axle H82-6217, including: side-view images of the replica profiles captured via optical microscopy, cross-sectional images at the deepest point of each notch, measured notch depths (covering a 10 mm arc segment centered at the deepest point), and quadratic curve fitting results of the deepest cross-sections. The depth values are obtained from the height measurements of the replica profile side views, calibrated accordingly.

The notch opening angles, notch tip radii of curvature, and stress concentration factors at the deepest points of the eight V-shaped notch locations were obtained through measurements of the replica sample profiles. For the notch shown in Figure 5, the notch opening angle is 77.2°. The notch depth comes to 1.053 mm, and the notch root radius of curvature is 0.393 mm. Then the stress concentration factor can be calculated as 4.19.

After 1.02×10^7 fatigue loading cycles, Axle H82-6217 experienced wheel hub disengagement, leading to the termination of the experiment. Magnetic particle inspection revealed that no cracks were observed in any of the eight artificially notched arc segments.

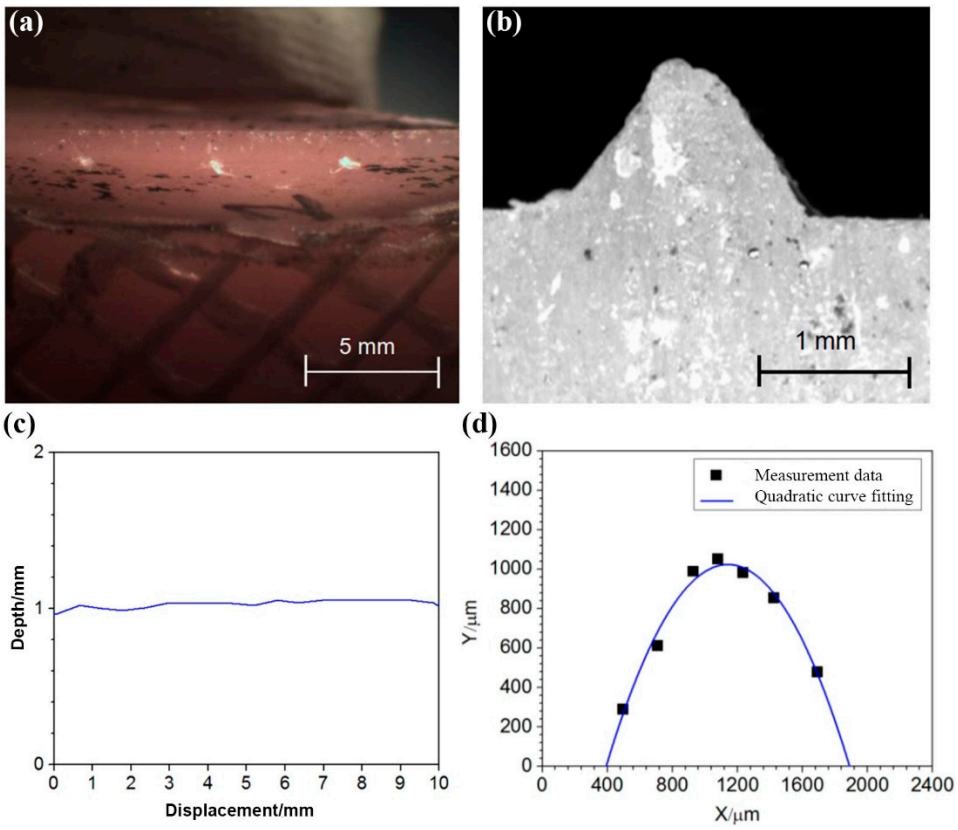

Figure 5. 1st round deepened notch on Axle H82-6217: (a) side-view optical observation of the notch, (b) notch replica profile, (b) measurement of the notch depth, and (c) quadratic curve fitting.

3.3. 3rd Round Fatigue Test and Results (Notch Further Deepened)

The existing eight notches on Axle H31-6201 were further deepened using a riffler file, with a target maximum notch depth of 1.5 mm. The maximum nominal bending stress at the notch location was calculated to be 238.5 MPa.

 doi:10.20944/preprints202507.0178.v1

Figure 6 presents the analysis results for one of the eight notches on Axle H31-6201. Following the same ways as above, the depth values for all eight notch locations (based on the 10 mm arc segments centered at the deepest points) were derived from the height measurements of the side-view replica profiles, calibrated accordingly. For the notch shown in Figure 6, the notch opening angle is 59.5°. The notch depth measures 1.760 mm, and the notch root radius of curvature is obtained as 0.310 mm. The stress concentration factor is therefore 5.49 as calculated.

After 1.96×10^6 fatigue loading cycles, Axle H31-6201 experienced axle disengagement. Magnetic particle inspection confirmed that no cracks were observed in any of the eight artificially notched arc segments.

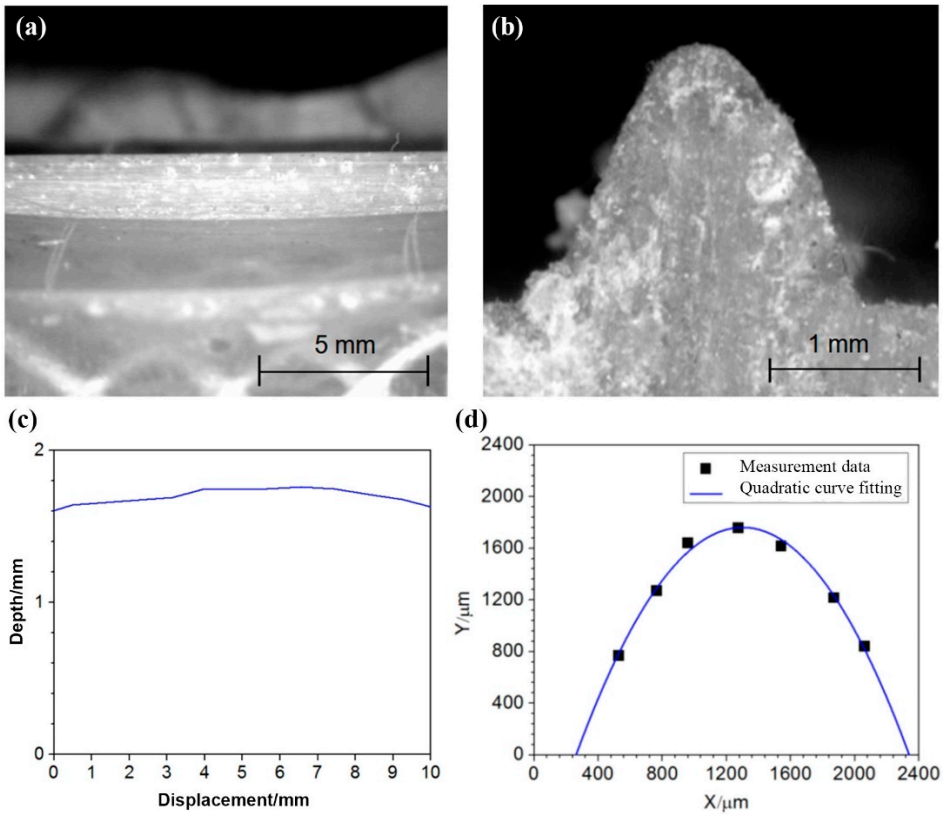

Figure 6. 2nd round deepened notch on Axle H31-6201: (a) side-view optical observation of the notch, (b) notch replica profile, (b) measurement of the notch depth, and (c) quadratic curve fitting.

4. Discussion

After the first round of testing, both the two axles containing circumferential V-shaped notches withstood 2×10^7 cycles of fatigue loading under a maximum applied stress of 240 MPa at the wheel seat, with no cracks detected at the artificial notches through magnetic particle inspection. In the second round, Axle H82-6217 experienced axle disengagement after 1.02×10^7 cycles, but again, no cracks were observed in the notched segments. In the third round, Axle H31-6201 disengaged after 1.96×10^6 cycles, and the test was terminated. No cracks were found in the notch segments.

Although notches are generally known to significantly reduce fatigue strength, the artificially prefabricated notches used in this study were sharper than typical fretting or impact-induced surface damage observed in service. For instance, the circumferential V-shaped notches prefabricated on the two axles reached a maximum depth of 0.669 mm and a maximum SCF of 3.12. The maximum nominal bending stress at the V-shaped notch, excluding notch effects, was 220.2 MPa, corresponding to a maximum local stress of 687.0 MPa when stress concentration is considered. Similarly, among the eight notches located 15 mm from the wheel seat on Axle H31-6201, the maximum notch depth was 0.906 mm, and the maximum SCF reached 4.54. The nominal bending stress at this location was

 doi:10.20944/preprints202507.0178.v1

238.5 MPa, which results in a maximum local stress of 1082.8 MPa when accounting for stress concentration. Despite these sharp prefabricated notches, no cracks were observed at any of the notch sites after 2×10^7 fatigue cycles, as verified by magnetic particle inspection. This clearly demonstrates the excellent fatigue resistance of the axle shaft material.

It is important to note that the fatigue strength of notched specimens is not solely determined by the local maximum stress at the notch root. Fatigue limit testing of S38C material—with surface hardness and low-temperature tempered martensitic microstructure like that of the axle surface—was conducted previously using the staircase method under rotating bending loading for 10^8 cycles. The results indicated that, under a 1% failure probability with 95% confidence, the lower bound of the fatigue strength for small specimens was 647 MPa, which is significantly lower than the maximum local stress of 1082.8 MPa estimated for the experimental axle with notch-induced stress concentration. Therefore, the fatigue strength of notched components cannot be accurately represented by simply referencing the local maximum stress near the notch root. Thus, estimating fatigue strength based on the maximum stress at the notch root in notched specimens is non-conservative. In contrast, estimating allowable notch severity based on the fatigue strength of unnotched specimens is conservative. This distinction underscores the need for comprehensive experimental validation rather than relying solely on local stress values in fatigue assessments of notched components.

5. Conclusions

In accordance with the EN 13261 standard, fatigue tests were conducted on actual axles with prefabricated notches under a maximum applied stress of 240 MPa at the wheel seat, with a stress ratio of $R = -1$. The key experimental findings are summarized as follows:

1. Two actual axles with circumferential V-shaped notches located 130 mm from the wheel seat—having notch depths of 0.572 mm, and 0.538 mm, and corresponding stress concentration factors of 2.48, and 2.53, respectively—underwent 2×10^7 cycles of fatigue loading. Magnetic particle inspection revealed no cracks along the circumferential notch segments.
2. On Axle H82-6217, the original circumferential V-shaped notch was deepened at eight positions, resulting in notch depths ranging from 0.968 to 1.132 mm and stress concentration factors between 4.12 and 4.84. After 1.02×10^7 cycles of fatigue loading, no cracks were detected at any of the notched arc segments by magnetic particle inspection.
3. On Axle H31-6201, eight chordal notches located 15 mm from the wheel seat, with notch depths between 0.709 and 0.906 mm and stress concentration factors from 3.49 to 4.54, were subjected to 2×10^7 fatigue cycles. No cracks were observed at any of the artificially notched arc segments.

These experimental results demonstrate that high-speed train axles with various prefabricated surface notches exhibit excellent fatigue resistance. Furthermore, the findings suggest that the existing overhaul specification limits—stipulating a maximum allowable impact depth of 0.3 mm and a scratch depth of 0.1 mm—may be conservatively low and could be appropriately relaxed based on experimental evidence.

Conflicts of Interest: The authors declare no conflicts of interest.

References

1. Glossary: High-speed rail. Available online: https://ec.europa.eu/eurostat/statistics-explained/index.php?title=Glossary:High-speed_rail (accessed on April 6, 2025).
2. High-speed rail. Available online: https://en.wikipedia.org/wiki/High-speed_rail (accessed on April 6, 2025).
3. Ollivier, G.; Bullock, R.; Jin, Y.; Zhou, N. *High-Speed Railways in China: A Look at Traffic*; World bank: Washington, DC, USA, 2014.

 doi:10.20944/preprints202507.0178.v1

4. Zerbst, U.; Klinger, C.; Klingbeil, D. Structural assessment of railway axles - A critical review. *Eng. Fail. Anal.* **2013**, *35*, 54–65.
5. Cong, T.; Qian, G.; Zhang, G.; Wu, S.; Pan, X.; Du, L.; Liu, X. Effects of inclusion size and stress ratio on the very-high-cycle fatigue behavior of pearlitic steel. *Int. J. Fatigue* **2021**, *142*, 105958.
6. Tong, Y.Y.; Liu, G.X.; Yousefian, K.; Jing, G.Q. Track Vertical Stiffness -Value, Measurement Methods, Effective Parameters and Challenges: A review. *Transp. Geotech.* **2022**, *37*, 100833.
7. Pan, X.; Qian, G.; Wu, S.; Fu, Y.; Hong, Y. Internal crack characteristics in very-high-cycle fatigue of a gradient structured titanium alloy. *Sci. Rep.* **2020**, *10*, 4742.
8. Yu, M.; Duquesnay, D.; Topper, T. Notch fatigue behavior of SAE1045 steel. *Int. J. Fatigue* **1988**, *10*, 109–116.
9. Chapetti, M.D.; Tagawa, T.; Miyata, T. Fatigue notch sensitivity of steel blunt-notched specimens. *Fatigue Fract. Eng. Mater. Struct.* **2002**, *25*, 629–634.
10. Verreman, Y.; Limodin, N. Fatigue notch factor and short crack propagation. *Eng. Fract. Mech.* **2008**, *75*, 1320–1335.
11. Jiang, Q.; Sun, C.; Liu, X.; Hong, Y. Very-high-cycle fatigue behavior of a structural steel with and without induced surface defects. *Int. J. Fatigue* **2016**, *93*, 352–362.
12. Lagoda, T.; Bilous, P.; Blacha, L. Investigation on the effect of geometric and structural notch on the fatigue notch factor in steel welded joints. *Int. J. Fatigue* **2017**, *101*, 224–231.
13. Zhang, C.; Yang, S.; Dong, Y.; Mu, S.; Li, H.; Zhang, J. Fatigue limit prediction of cracked and notched specimens related to grain size. *Int. J. Fatigue* **2023**, *177*, 107905.
14. Hwang, D.; Cho, S.S. Correlation between fretting and plain fatigue using fatigue damage gradient. *J. Mech. Sci. Technol.* **2014**, *28*, 2153–2159.
15. Li, X.; Zuo, Z.; Qin, W. A fretting related damage parameter for fretting fatigue life prediction. *Int. J. Fatigue* **2015**, *73*, 110–118.
16. Huang, Z.; Zhang, Z.; Teng, Z.; Khan, M.K.; Wang, Q.; Wang, J. Effect of fretting damage on characteristics of high strength bearing steel up to very high cycle fatigue. *Eng. Fract. Mech.* **2019**, *217*, 106526.
17. Wang, X.; Ping, X.; Zeng, X.; Wang, R.; Zhao, Q.; Ying, S.; Hu, T. Fretting fatigue experiment and simulation of WC-12Co coating taking into account the wear effects. *Surf. Coat. Technol.* **2022**, *441*, 128555.
18. Cavuto, A.; Martarelli, M.; Pandarese, G.; Revel, G.M.; Tomasini, E.P. Experimental investigation by Laser Ultrasonics for train wheelset flaw detection. *J. Phys. Conf. Ser.* **2018**, *1149*, 012015.
19. Pathak, M.; Alahakoon, S.; Spiryagin, M.; Cole, C. Rail foot flaw detection based on a laser induced ultrasonic guided wave method. *Measurement* **2019**, *148*, 106922.
20. Wang, Y.W.; Ni, Y.Q.; Wang, X. Real-time defect detection of high-speed train wheels by using Bayesian forecasting and dynamic model. *Mech. Syst. Signal Process.* **2020**, *139*, 106654.
21. Pan, X.; Su, H.; Sun, C.; Hong, Y. The behavior of crack initiation and early growth in high-cycle and very-high-cycle fatigue regimes for a titanium alloy. *Int. J. Fatigue* **2018**, *115*, 67–78.
22. Pan, X.; Hong, Y. High-cycle and very-high-cycle fatigue behaviour of a titanium alloy with equiaxed microstructure under different mean stresses. *Fatigue Fract. Eng. Mater. Struct.* **2019**, *42*, 1950–1964.
23. Pan, X.; Su, H.; Liu, X.; Hong, Y. Multi-scale fatigue failure features of titanium alloys with equiaxed or bimodal microstructures from low-cycle to very-high-cycle loading numbers. *Mater. Sci. Eng. A* **2024**, *890*, 145906.
24. EN 13261. *Railway applications - Wheelsets and bogies - Axles - Product requirements*; European Committee for Standardization: Brussels, Belgium, 2023.
25. Schijve, J. *Fatigue of Structures and Materials*, 2nd ed.; Springer: Dordrecht, Germany, 2009.

 doi:10.20944/preprints202507.0178.v1

26. Sun, J.Y.; Zhao, X.; Illeperuma, W.R.K.; Chaudhuri, O.; Oh, K.H.; Mooney, D.J.; Vlassak, J.J.; Suo, Z. Highly stretchable and tough hydrogels. *Nature* **2012**, *489*, 133–136.
27. Jiang, Z.; Ji, Z.; Zhu, M.; Ma, W.; Gao, S.; Xu, M. Notch-insensitive, tough and self-healing conductive bacterial cellulose nanocomposite hydrogel for flexible wearable strain sensor. *Int. J. Biol. Macromol*. **2024**, *280*, 135947.
28. Zhao, C.; Wu, W.; Deng, J.; Yu, M.; Peng, Y.; Wang, X.; Gong, J. Hydrogen-induced delayed fracture behavior of notched 316L austenitic stainless steel: Role of grain refinement. *Eng. Fail. Anal.* **2024**, *166*, 108880.
29. Cicero, S. Assessment of structural materials containing notch-type defects: A comprehensive validation of the FAD-TCD methodology on metallic and non-metallic materials. *Theor. Appl. Fract. Mech*. **2024**, *133*, 104612.
30. Medina, L.; Díaz, A.; Rodriguez-Aparicio, R.; Mayoral, N.; Cuesta, I.I.; Alegre, J.M. Notch sensitivity analysis of a 2205 duplex stainless steel in a gaseous hydrogen environment. *Theor. Appl. Fract. Mech*. **2024**, *134*, 104655.
31. Wan, R.; Long, Z.; Cui, Y.; You, L. Strengthening effects of indentation notches on metallic glasses and their sensitivity to stress triaxiality. *J. Non-Cryst. Solids* **2024**, *645*, 123187.
32. Minerva, G.; Awd, M.; Koch, A.; Walther, F.; Beretta, S. Transferability of anomaly data to fatigue properties of PBF-LB AlSi10Mg parts with different volumes. *Int. J. Fatigue* **2025**, *195*, 108852.
33. Ahmad, N.; Irfan, S.; Maleki, E.; Lee, S.; Liu, J.P.; Shao, S.; Shamsaei, N. Determining critical surface features affecting fatigue behavior of additively manufactured Ti-6Al-4V. *Int. J. Fatigue* **2025**, *197*, 108956.
34. Kwon, O.; Lim, H.J.; Sohn, H. Reference-free remaining fatigue life prediction for notched aluminum 6061-T6 plates without preliminary fatigue tests. *Mech. Syst. Signal Process*. **2025**, *229*, 112569.
35. Kumar, A.; Jha, J.S.; Mishra, S.K.; Tandaiya, P. Effect of notch root radius on apparent fracture toughness of Ti6Al4V alloy: experiments and simulations. *Int. J. Fract*. **2025**, *249*, 7.
36. Boussahra, M.S.N.; Madani, K.; Benyettou, M.; Harmel, M.W.; Aminallah, S.; Zouggar, K.; Campilho, R.D.S.G. Novel patch shape for the repair of inclined cracks in DH 36 steel structures: Numerical analysis. *Mech. Adv. Mater. Struct*. **2025**, *in press*, DOI10.1080/15376494.2025.2507837
37. Zhang, S.; Xie, J.; Jiang, Q.; Zhang, X.; Sun, C.; Hong, Y. Fatigue crack growth behavior in gradient microstructure of hardened surface layer for an axle steel. *Mater. Sci. Eng. A* **2017**, *700*, 66–74.
38. Qin, T.; Hu, F.; Xu, P.; Zhang, H.; Zhou, L.; Ao, N.; Su, Y.; Shobu, T.; Wu, S. Gradient residual stress and fatigue life prediction of induction hardened carbon steel S38C axles: Experiment and simulation. *Int. J. Fatigue* **2024**, *185*, 108336.
39. Hu, F.; Qin, T.; Ao, N.; Su, Y.; Zhou, L.; Xu, P.; Parker, J.D.; Shinohara, T.; Chen, J.; Wu, S. Gradient residual strain determination of surface impacted railway S38C axles by neutron Bragg-edge transmission imaging. *Eng. Fract. Mech*. **2024**, *306*, 110267.
40. Hu, F.; Qin, T.; Su, Y.; He, L.; Ao, N.; Parker, J.D.; Shinohara, T.; Wu, S. Residual stress relaxation of railway gradient S38C steel during fatigue crack growth by neutron imaging and diffraction. *Int. J. Fatigue* **2025**, *193*, 108826.
41. Huang, M. *Analysis and research of fretting damage on wheel/rd2 axle interface*; Dissertation/Thesis. Chengdu, China, Southwest Jiaotong University, 2010.
42. Murakami, Y. Metal Fatigue: Effect of Small Defects and Nonmetallic Inclusions; Elsevier: Oxford, UK, 2002.

 doi:10.20944/preprints202507.0178.v1

43. Zerbst, U.; Beretta, S.; Köhler, G.; Lawton, A.; Vormwald, M.; Beier, H.T.; Klinger, C.; Cerny, I.; Rudlin, J.; Heckel, T.; Klingbeil, D. Safe life and damage tolerance aspects of railway axles - A review. *Eng. Fract. Mech.* **2013**, *98*, 214–271.
44. Sun, C.; Song, Q.; Zhou, L.; Pan, X. Characteristic of interior crack initiation and early growth for high cycle and very high cycle fatigue of a martensitic stainless steel. *Mater. Sci. Eng. A* **2019**, *758*, 112–120.
45. Chang, Y.; Zheng, L.; Pan, X.; Hong, Y. Further investigation on microstructure refinement of internal crack initiation region in VHCF regime of high-strength steels. *Frattura ed Integrità Strutturale* **2019**, *13(49)*, 1-11.
46. Pan, X.; Xu, S.; Qian, G.; Nikitin, A.; Shanyavskiy, A.; Palin-Luc, T.; Hong, Y. The mechanism of internal fatigue-crack initiation and early growth in a titanium alloy with lamellar and equiaxed microstructure. *Mater. Sci. Eng. A* **2020**, *798*, 140110.
47. Chang, Y.; Pan, X.; Zheng, L.; Hong, Y. Microstructure refinement and grain size distribution in crack initiation region of very-high-cycle fatigue regime for high-strength alloys. *Int. J. Fatigue* **2020**, *134*, 105473.
48. Qian, G.; Jian, Z.; Qian, Y.; Pan, X.; Ma, X.; Hong, Y. Very-high-cycle fatigue behavior of AlSi10Mg manufactured by selective laser melting: Effect of build orientation and mean stress. *Int. J. Fatigue* **2020**, *138*, 105696.
49. Pan, X.; Qian, G.; Hong, Y. Nanograin formation in dimple ridges due to local severe-plastic-deformation during ductile fracture. *Scr. Mater.* **2021**, *194*, 11363.
50. Du, L.; Pan, X.; Qian, G.; Zheng, L.; Hong, Y. Crack initiation mechanisms under two stress ratios up to very-high-cycle fatigue regime for a selective laser melted Ti-6Al-4V. *Int. J. Fatigue* **2021**, *149*, 106294.
51. Liu, L.; Ma, Y.; Liu, S.; Wang, S. The fatigue behaviors of a medium-carbon pearlitic wheel-steel with elongated sulfides in high-cycle and very-high-cycle regimes. *Materials* **2021**, *14(15)*, 4318.
52. Pan, X.; Du, L.; Qian, G.; Hong, Y. Microstructure features induced by fatigue crack initiation up to very-high-cycle regime for an additively manufactured aluminium alloy. *J. Mater. Sci. Technol.* **2024**, *173*, 247–260.
53. Pan, X.; Xu, S.; Nikitin, A.; Shanyavskiy, A.; Palin-Luc, T.; Hong, Y. Crack initiation induced nanograins and facets of a titanium alloy with lamellar and equiaxed microstructure in very-high-cycle fatigue. *Mater. Lett.* **2024**, *357*, 135769.
54. Du, L.; Pan, X.; Hong, Y. New insights into microstructure refinement in crack initiation region of very-high-cycle fatigue for SLM Ti-6Al-4V via precession electron diffraction. *Materialia* **2024**, *33*, 102008.
55. Tao, Z.; Wang, Z.; Pan, X.; Su, T.; Long, X.; Liu, B.; Tang, Q.; Ren, X.; Sun, C.; Qian, G.; et al. A new probabilistic control volume scheme to interpret specimen size effect on fatigue life of additively manufactured titanium alloys, *Int. J. Fatigue* **2024**, *183*, 108262.
56. Pan, X.; Hong, Y. High-cycle and very-high-cycle fatigue of an additively manufactured aluminium alloy under axial cycling at ultrasonic and conventional frequencies. *Int. J. Fatigue* **2024**, *185*, 108363.
57. Gao, C.; Zhang, Y.; Jiang, J.; Fu, R.; Du, L.; Pan, X. Research viewpoint on performance enhancement for very-high-cycle fatigue of Ti-6Al-4V alloys via laser-based powder bed fusion. *Crystals* **2024**, *14(9)*, 749.
58. Tao Z.; Chang, Y.; Pan, X.; Qian, G.; Hong, Y. Numerical simulation of crack surface contacting behavior with stress-induced martensitic phase transformation in very-high-cycle fatigue regime. *Int. J. Fatigue* **2025**, *198*, 109019.
59. Pan, X.; Tao, Z.; Long, X. Extraordinary specimen-size effect on long-life fatigue of additively manufactured AlSi10Mg. *Int. J. Mech. Sci.* **2025**, *301*, 110524.
60. Tan, X.; Kok, Y.; Tan, Y.J.; Descoins, M.; Mangelinck, D.; Tor, S.B.; Leong, K.F.; Chua, C.K. Graded microstructure and mechanical properties of additive manufactured Ti-6Al-4V via electron beam melting. *Acta Mater.* **2015**, *97*, 1–16.

 doi:10.20944/preprints202507.0178.v1

61. Fu, Z.K.; Ding, H.H.; Wang, W.J.; Liu, Q.Y.; Guo, J.; Zhu, M.H. Investigation on microstructure and wear characteristic of laser cladding Fe-based alloy on wheel/rail materials. *Wear* **2015**, *330*, 592–599.
62. DebRoy, T.; Wei, H.L.; Zuback, J.S.; Mukherjee, T.; Elmer, J.W.; Milewski, J.O.; Beese, A.M.; Wilson-Heid, A.; De, A.; Zhang, W. Additive manufacturing of metallic components—Process, structure and properties. *Prog. Mater. Sci.* **2018**, *92*, 112–224.
63. Qian, G.; Jian, Z.; Pan, X.; Berto, F. In-situ investigation on fatigue behaviors of Ti-6Al-4V manufactured by selective laser melting. *Int. J. Fatigue* **2020**, *133*, 105424.
64. Long, X.; Jia, Q.; Li, J.; Chong, K.; Du, L.; Pan, X.; Chang, C. Mechanical properties and parameter optimization of TC4 alloy by additive manufacturing. *China Surf. Eng.* **2022**, *35*, 215–223. (in Chinese)
65. Badoniya, P.; Srivastava, M.; Jain, P.K.; Rathee, S. A state-of-the-art review on metal additive manufacturing: Milestones, trends, challenges and perspectives. *J. Braz. Soc. Mech. Sci*. **2024**, *46*, 339.
66. Xu, S.; Pan, S.; Li, Z.; Li, S.; He, X.; Pan, X. Anisotropic tensile behavior and fracture characteristics of an additively manufactured nickel alloy without and with a heat treatment of solution aging. *Mater. Sci. Eng. A* **2025**, *927*, 148015.